A rapidly metabolizable and enzyme-activated NIR fluorescent probe based on isophorone for imaging in vivo

Wenxin Kang [a], Mo Ma [a,b], Shuai Tang [c], Yuning Wang [a], Jingkang Li [a], Lanlan Xu [a], Pinyi Ma [a], Daqian Song [a], Ying Sun [a,*]

[a] College of Chemistry, Jilin Province Research Center for Engineering and Technology of Spectral Analytical Instruments, Jilin University, Qianjin Street 2699, Changchun 130012, China
[b] College of Pharmacy, Jilin University, Qianjin Street 2699, Changchun 130012, China
[c] College of Chemistry, Jilin University, Qianjin Street 2699, Changchun 130012, China

ARTICLE INFO

ABSTRACT

Near-infrared (NIR) fluorescent probes have excellent properties such as fast imaging speed, non-invasive, good stability and low background interference, and have great application potential in biological imaging and surgical guidance. At present, the study of fluorescent probes with long time imaging has attracted extensive attention to guide surgery, while some issues need to be considered, such as toxicity, long tissue residence time and long time for metabolism. Meanwhile, fluorescent probes with rapid metabolism tend to decay fast. Therefore, fluorescent probes need to be continuously designed and synthesized to achieve a balance of performance between suitable imaging time and reasonable metabolic rate. To this end, we design a NIR fluorescence probe that can not only complete the needs of in vivo or cell imaging in a reasonable time, but also can rapidly metabolize and shorten its residence time in the body. The synthesis of a rapidly metabolizable NIR fluorescent probe Kang-CES2 were based on isophorone for enzyme-activated imaging anaplastic thyroid cancer (ATC) in vivo. Kang-CES2 has demonstrated excellent imaging capabilities in vivo and potentiality as a spray and biopsies tool. Meanwhile, the results of intratumoral injection in mice showed that Kang-CES2 can quickly distinguish between normal and ATC tissues and continue to emit NIR light until the end of surgery. The results of tail vein injection of mice showed that Kang-CES2 can rapidly metabolize in the body within 33 minutes. We believe Kang-CES2 has the potential to be a powerful fluorescent tool capable of guiding ATC surgical resection with rapid metabolism.

1. Introduction

At present, fluorescent probes have good application potential in bioimaging[1,2]. Fluorescent probes can monitor many physiological and pathological processes in real time at the cellular or even molecular level, and play an increasingly important role in clinical surgery[3–6]. In particular, the near-infrared fluorescent probe has excellent properties such as fast imaging speed, non-invasive, good stability and small background interference[7,8]. Especially, isophorone-based fluorescent probes have attracted much attention due to their advantages of easy synthesis, excellent performance and large Stokes shift[9–14]. A number of fluorescent probes have been reported that can be used to guide imaging during surgery[11,14–17]. Among them, some fluorescent probes that can image over a long period of time have attracted much attention, such as,

such as, long-term specific cancer cell membrane imaging fluorescence probe reported by Fu et al.[18], long-term cell imaging fluorescence probe reported by Li et al.[19], ultra-high-intensity fluorescence probe reported by Xu et al.[20]. However, there are still some limitations that should be considered such as toxicity, long tissue residence time and long time for metabolism, when fluorescent probes are used as ultra-long-term imaging tools to guide surgery[21–26]. Meanwhile, fluorescent probes with rapid metabolism tend to decay fast[27–32]. Therefore, fluorescent probes need to be continuously designed and synthesized to achieve a balance of performance between suitable imaging time and reasonable metabolic rate. To overcome this challenge, we are committed to design a NIR fluorescent probe that can both fulfill the need for in vivo or cell imaging in a reasonable time, and rapidly metabolize to shorten its residence time in the body. We hope to apply

this probe to the detection and imaging of thyroid cancer to provide a safer and more promising chemical sensor for clinical surgical guidance of thyroid cancer.

The incidence of thyroid cancer has always been high, and severe thyroid cancer can lead to a high mortality rate[33]. ATC as a malignant thyroid cancer, people are exploring a variety of treatment methods, including total resection, radiation therapy and radiotherapy combined therapy[34,35]. Surgery is still the most commonly used treatment. If normal tissue and malignant tissue can be accurately distinguished during surgical resection, the recurrence of disease caused by incomplete resection can be effectively avoided and the function of the organ can be preserved to the maximum extent. Therefore, it is critical to develop a near-infrared fluorescent probe that can accurately distinguish ATC tumors. Mammalian carboxylesterase (CESs) is a key enzyme in the serine hydrolase family, which is involved in important life activities of human body[36–38]. Carboxylesterase 2 (CES2) is mainly distributed in the small intestine, liver, thyroid and kidney, and is closely related to many types of cancer[39–46]. It is worth noting that the expression level of CES2 is not same in normal cells and cancer cells in different tissues, and usually high expression level in cancer cells is more conducive to subsequent in vivo imaging experiments[47–49]. It has been reported that CES2 expression is higher in thyroid tumor tissue than in normal thyroid tissue, so follow-up imaging experiments can be designed with fluorescent probes that respond specifically to CES2 [50–52]. To date, organic small molecule fluorescent probes for thyroid cancer detection are still in the exploratory stage[52–56], and the balance between imaging duration and metabolism has not been reported.

Here, we report the design and synthesis of a rapidly metabolizable enzyme-activated NIR fluorescent probe based on isophorone. Kang-CES2 can respond specifically to CES2 in vitro and in vivo, image fast, metabolize rapidly and emit NIR light. Kang-CES2 also has good photostability, selectivity, low cytotoxicity, good biosafety and can quantitatively detect CES2 in the range of 0–0.40 µg/mL. The sensing mechanism of Kang-CES2 to CES2 was investigated by HPLC analysis, LC-HRMS analysis, cyclic voltammetry (CV) test and molecular docking simulation. Through the experimental results of the above tests, we demonstrated that CES2 can cut the ester bond of Kang-CES2 and restore it to fluorophore DIPCl-OH. Besides these, Kang-CES2 also demonstrates excellent imaging capabilities in vivo imaging and its potential as a spray tool and biopsies tool. The results of intratumoral injection in mice showed that Kang-CES2 can quickly distinguish between normal and ATC tissues and continue to emit NIR light until the end of surgery. In addition, by injecting Kang-CES2 into the tail vein of normal mice, imaging results showed that Kang-CES2 can be rapidly metabolized in vivo within 33 minutes. The performance of Kang-CES2 achieves the balance of imaging ATC tissue at a reasonable time covering surgical duration of ATC[57] and enabling rapid metabolism. We believe Kang-CES2 has the potential to be a powerful fluorescent tool capable of guiding ATC surgical resection and rapid metabolism.

2. Experimental section

2.1. Synthesis route

Fig. 1A shows the synthesis route of Kang-CES2 (refer to support information for detailed synthesis methods). In addition, Fig. S1-8 shows the necessary spectra of compound 1, DIPCl-OH and Kang-CES2 (including ^1H NMR, ^{13}C NMR and MS spectra).

2.2. Recording of spectra

Ultraviolet-visible (UV–VIS) spectra and fluorescence spectra of different concentrations of CES2 and Kang-CES2 were recorded after incubation at 37 ℃. Among them, it includes condition optimization, performance testing and selective testing. The probe concentration in the mixture used for testing was 10 µM. The preparation method was to prepare 1.0 mM cell mother liquor by adding Kang-CES2 to dimethyl sulfoxide (DMSO), and then dilute it to 1.0 mL in PBS. The UV absorption peaks and fluorescence emission peaks of DIPCl-OH and Kang-CES2 were obtained in the spectral test at first (Fig. 1B and C). The UV absorption peak of DIPCl-OH was 420 nm, and the fluorescence emission peak was 698 nm. The UV absorption peak of Kang-CES2 is 390 nm, and there is no obvious fluorescence emission peak. The fluorescence quantum yield of DIPCl-OH is 5.11 %.

3. Results and discussions

3.1. Performance test

The reaction between Kang-CES2 and CES2 was preliminarily analyzed by spectroscopic method. The UV absorption spectrum of Kang-CES2 and CES2 mixture has a UV absorption peak at 420 nm, which is the same position as the UV absorption peak of fluorophore DIPCl-OH (Fig. 1B). The fluorescence spectra of the mixture showed a
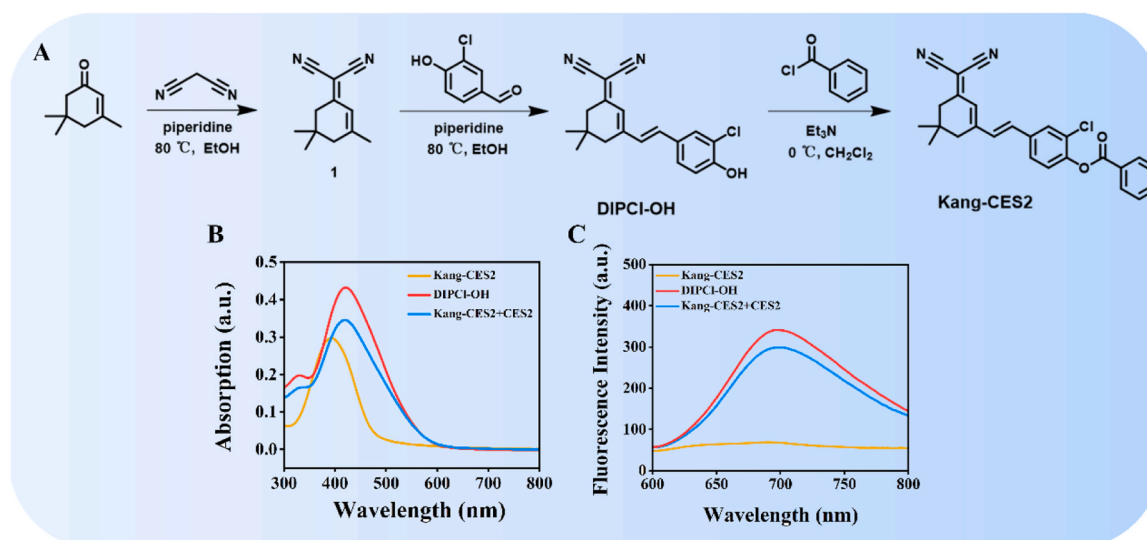

Fig. 1. (A) Synthesis route of Kang-CES2; (B) UV–VIS spectra of 10 µM DIPCl-OH, 10 µM Kang-CES2 + 1.00 µg/mL CES2, 10 µM Kang-CES2; (C) fluorescence curves of 10 µM DIPCl-OH, 10 µM Kang-CES2 + 1.00 µg/mL CES2, 10 µM Kang-CES2.

strong fluorescence emission peak at 698 nm, which was the same as that of the fluorophore DIPCl-OH (Fig. 1C). The results show that the reaction of Kang-CES2 with CES2 can be reduced to DIPCl-OH.

Subsequently, we optimized the reaction conditions of Kang-CES2 to detect CES2. In the optimization of reaction time, we found that the fluorescence intensity of Kang-CES2 and CES2 reaction mixtures increased with the extension of incubation time and stabilized after 60 min (Fig. 2D). Therefore, 60 min was determined as the incubation time for subsequent experiments. Notably, the reaction time of Kang-CES2 was significantly higher than that of a probe with similar structure without chlorine atom (Table. S1). This result may be due to the addition of chlorine atom, which reduces the molecular electron cloud density and makes the structure more stable. In summary, Kang-CES2 has the potential to maintain reasonable imaging times, including the duration of ATC surgery.

In the light stability test, the fluorescence signal of Kang-CES2, DIPCl-OH and reaction system (Kang-CES2 + CES2) did not change significantly after continuous laser irradiation, indicating that all substances in the experiment have good light stability (Fig. 2F). In addition, the effects of pH on Kang-CES2, DIPCl-OH and reaction system were also tested (Fig. 2G). When pH is less than 6, the fluorescence intensity is lower. When pH is greater than 6, the reaction system is gradually affected with the increase of pH. The fluorescence intensity of DIPCl-OH and the fluorescence intensity of the reaction system reached a balance point at pH 7.4. Therefore, considering the experimental results and the pH value (7 or 7.4) of the currently accepted in vitro detection, the pH of in vitro test was determined to be 7.4. In addition, the pK_a of DIPCl-OH is 8.1 by Boltzmann constant fitting (Fig. S9).

We analyzed the fluorescence spectra of Kang-CES2 and different concentrations of CES2 after incubation at 37 °C for 60 min. The fluorescence intensity of the mixture at 698 nm increased with the increase of CES2 concentration (0–1.00 μg/mL), as shown in Fig. 2A, and the curve relationship was shown in Fig. 2B. There was a good linear

relationship between CES2 concentration at 698 nm and CES2 fluorescence at 0–0.40 μg/mL ($R^2 = 0.9949$) (Fig. 2C). Kang-CES2 can detect and quantify CES2 at 0–1.00 μg/mL, and the detection limit can be calculated as low as 0.0014 μg/mL by LOD = 3σ/k, indicating that Kang-CES2 has high sensitivity in CES2 detection. Compared with other reported CES2-activated probes, Kang-CES2 has the advantage of low detection limit and large Stokes shift (Table. S2). Finally, we evaluated the selectivity of Kang-CES2 to CES2. Selective testing includes more than 40 potentially interfering substances such as cations, anions, proteins and enzymes. We found that there was no significant fluorescence enhancement between each group of interfering substances and the blank group (Fig. 2E). The results show that Kang-CES2 has strong anti-interference ability and high selectivity to CES2. At the same time, the results indicate that Kang-CES2 has the potential for further application in vivo.

3.2. Sensing mechanism

The sensing mechanism of Kang-CES2 and CES2 inspires us to explore the interaction between Kang-CES2 and CES2. We inferred through spectral experiments and experience that CES2 can cut the ester bond of Kang-CES2 and restore it to fluorophore DIPCl-OH (Fig. 3A). Firstly, the retention times of each substance were analyzed by HPLC (Fig. 3B). The results showed that the retention time of Kang-CES2 and DIPCl-OH was 3.33 min and 1.63 min respectively. After CES2 is added, two retention times appear in the system, which are 1.63 min and 3.33 min respectively, corresponding to Kang-CES2 and DIPCl-OH. In order to further verify the sensing mechanism, we verified it by LC-HRMS analysis (Fig. S10). LC-HRMS analysis showed that the mass spectrum peaks of Kang-CES2 and CES2 reaction systems at different retention times were consistent with those of Kang-CES2 and DIPCl-OH.

By testing the CV curve, we found that DIPCl-OH has a characteristic oxidation peak, but the signal of Kang-CES2 is not obvious (Fig. 3C).
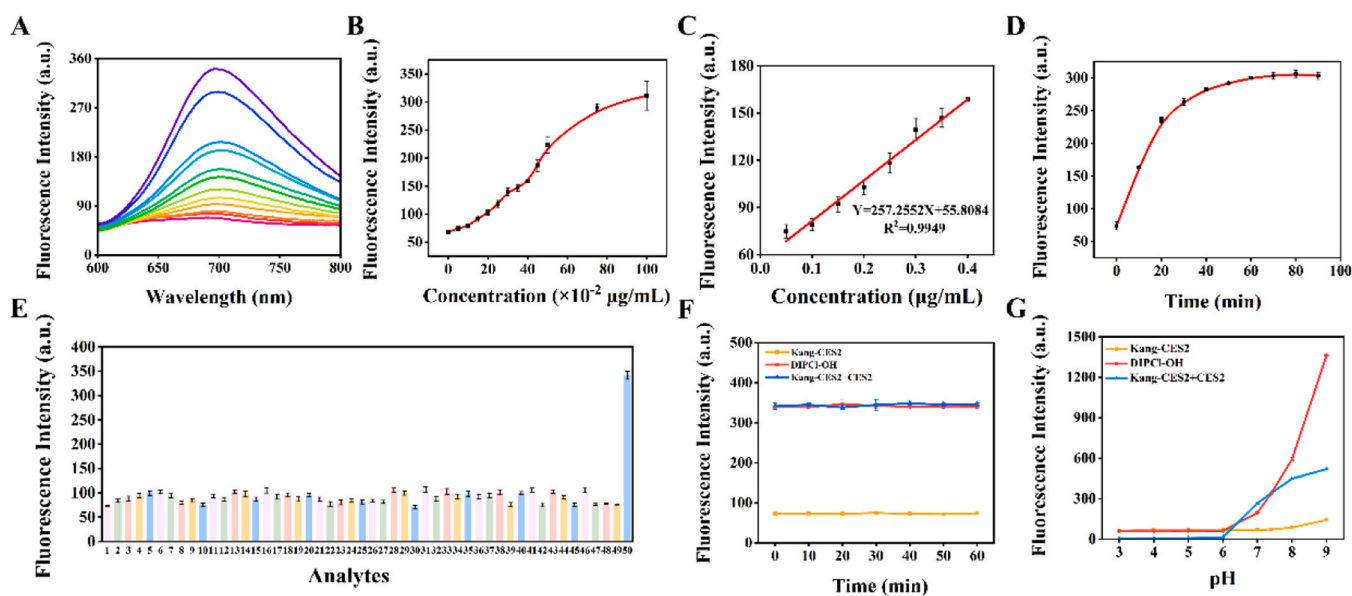

Fig. 2. Kang-CES2 performance test. (A) Fluorescence spectra of 10 μM Kang-CES2 with different CES2 concentration (0–1.00 μg/mL); (B) fluorescence spectra of 10 μM Kang-CES2 reacting with different concentration of CES2 (0–1.00 μg/mL); (C) linear curves of 10 μM Kang-CES2 with different CES2 concentration (0–0.40 μg/mL); (D) fluorescence intensity curves of 10 μM Kang-CES2 + 1.00 μg/mL CES2 at different times (0–90 min); (E) fluorescence intensity of different interfering substances reacting with 10 μM Kang-CES2. 1. blank (10 μM Kang-CES2); 1 mM cation: 2.Al^{3+}; 3.Ba^{2+}; 4.Ca^{2+}; 5.Cd^{2+}; 6.Co^{2+}; 7.Cu^{2+}; 8.Fe^{3+}; 9.K^+; 10.Li^+; 11.Mg^{2+}; 12.Na^+; 13.Mn^{2+}; 14.Pb^{2+}; 1 mM anion: 15.ClO_4^-; 16.HSO_4^-; 17. AcO^-; 18. CN^-; 19. I^-; 20. F^-; 21. $H_2PO_4^-$; 22. Br^-;23. Cl^-; 24. SCN^-; 25.SO_3^{2-}; 1 mM amino acid: 26. Ile; 27. L-Leu; 28. L-Ala; 29. Val; 30. Lys; 31. Asn; 32. Gly; 33.AsA; 34. Glu; 35. Phe; 36. L-His; 37. L-Pro; 38. L-Thr; 39. L-Arg; 40. L-Cys; 41. DL-HCY; 42. protein; Enzyme (1000 U/L): 43. β-glu; 44. β-gal; 45. APN; 46. LAP; 47. AChE; 48. BChE; Enzyme (1.00 μg/mL): 49. CES1; 50. CES2; (F) photostability test of 10 μM Kang-CES2, 10 μM DIPCl-OH, 10 μM Kang-CES2 + 1.00 μg/mL CES2; (G) fluorescence intensity curves of 10 μM Kang-CES2, 10 μM DIPCl-OH, 10 μM Kang-CES2 + 1.00 μg/mL CES2 incubated for 60 min at different pH (3−9). All samples were incubated for 60 min. The error bar represents calculating the mean ±SEM in three measurements. $\lambda_{ex/em} = 555/698$ nm.
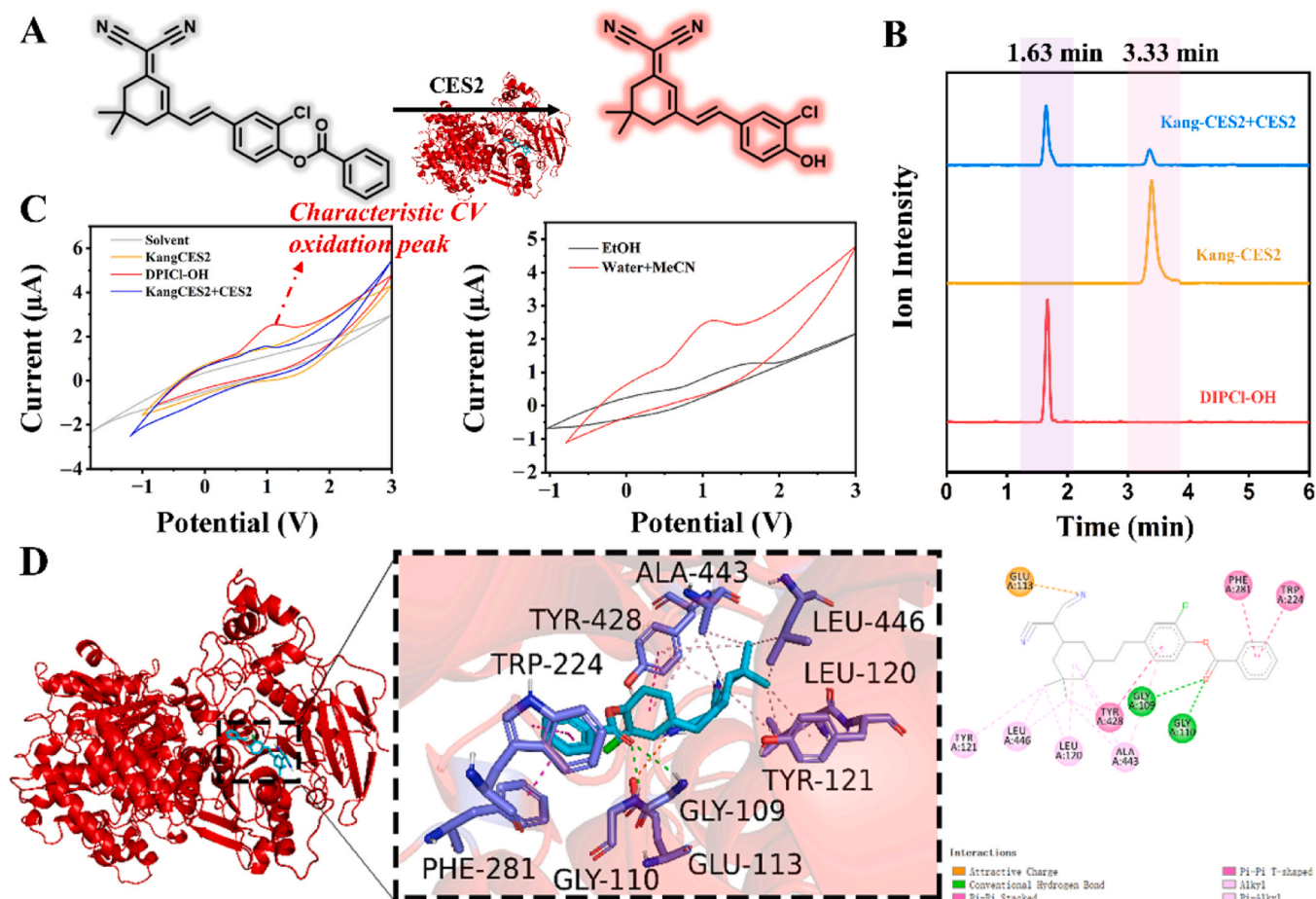
Fig. 3. Sensing mechanism. (A) Possible sensing mechanism; (B) HPLC analysis of 10 μM Kang-CES2, 10 μM DIPCl-OH, 10 μM Kang-CES2 + 1.00 μg/mL CES2; (C) CV curves of 10 μM Kang-CES2, 10 μM DIPCl-OH, 10 μM Kang-CES2 + 1.00 μg/mL CES2 in the mixture of water and acetonitrile (left) and 10 μM DIPCl-OH in different solvents (right); (D) molecular docking simulation of Kang-CES2 and CES2.

When Kang-CES2 reacted with CES2, the system also showed an oxidation peak similar to that of DIPCl-OH. When Kang-CES2 reacted with CES2, the oxidation peak of Kang-CES2 was similar to that of DIPCl-OH, which verified the sensing mechanism again. It is worth noting that Kang-CES2 showed no obvious signal in CV test, while the fluorophore DIPCl-OH and reaction system showed oxidation signal, suggesting that the probe has the potential of electro-fluorescence dual signal detection in vitro. In addition, we also explored the CV curve of DIPCl-OH in different solvents, which showed that DIPCl-OH exhibited similar characteristic oxidation peaks in both water and acetonitrile mixtures and ethanol. Finally, we demonstrated the binding of Kang-CES2 and CES2 with a binding energy of −10.7 kcal/mol through molecular docking simulation (Fig. 3D). This result shows that CES2 can effectively recognize Kang-CES2. All the above results expounded the mechanism of Kang-CES2 interaction with CES2 is that the ester bond is severed and the fluorophore DIPCl-OH is restored.

3.3. Biosecurity test

The cytotoxicity of Kang-CES2 was evaluated by CCK88 method before applying it to live cell CES2 imaging. When the concentration of Kang-CES2 was increased to 100 μM for 24 h, the cell viability was still higher than 92 % (Fig. S11A), indicating that Kang-CES2 has low cytotoxicity and can be used for cell imaging. Subsequently, we confirmed that Kang-CES2 had low toxicity to red blood cells and good blood compatibility through hemolysis experiments. As shown in Fig. S11B, the deionized water group showed red transparency, while the other groups showed clear and transparent supernatant. Although the

hemolysis rate increased with the increase of Kang-CES2 concentration, even when the concentration was increased to 50 μM, the hemolysis rate was only 1.5 %, below the standard threshold of 5 %. These assay results demonstrated that Kang-CES2 has excellent biosecurity.

3.4. Cellular endogenous CES2 imaging

In this study, two human cell lines were used, being ATC cells (C643) and normal thyroid cells (Nthy-ori3–1). The fluorescence of Kang-CES2 in normal thyroid cells was observed over time to optimize the cell experiment time, and fluorescence appeared almost immediately after intracellular incubation with Kang-CES2 (Fig. S12). The intracellular fluorescence intensity increased gradually with the increase of time, and basically reached the plateau at 4 h. At the same time, 4 h was selected as the best incubation time. Next, we explored the ability of Kang-CES2 to display endogenous CES2 in vitro. The Nthy-ori3–1 and C643 cells could be divided into four groups for processing and the imaging results compared. The first group was a blank control group with only Nthy-ori3–1 cells and C643 cells. The second group was the probe incubation group in Nthy-ori3–1 cells and C643 cells. The third group of C643 cells was incubated with 1 mM 5-fluorouracil (5-FU, CES2-activator) for 1 h, washed with PBS and incubated with 10 μM Kang-CES2 for 4 h. In the fourth group, C643 cells were incubated with 1 mM loperamide (LPA, CES2-inhibitor) for 1 h, washed with PBS and incubated with 10 μM Kang-CES2 for 4 h.

Fig. 4A shows the cell imaging results. First, the fluorescence signal of the cells after adding Kang-CES2 was compared with the control group (a) and (c), Nthy-ori3–1 cells group (b) and C643 cells group (d).
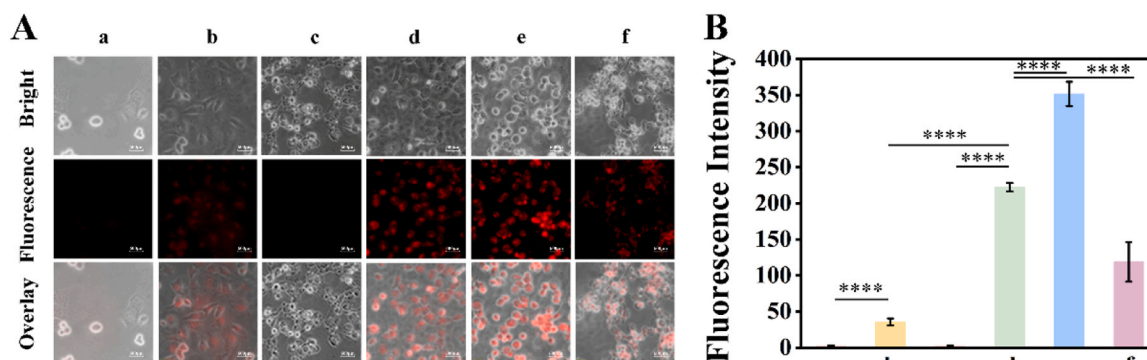
Fig. 4. (A) Fluorescence images of 10 μM Kang-CES2 in different treated cells: (a) Nthy-ori3–1 cells (blank); (b) Nthy-ori3–1 cells+10 μM Kang-CES2 for 4 h; (c) C643 cells (blank); (d) C643 cells+10 μM Kang-CES2 for 4 h; (e) C643 cells+1 mM 5-Fu for 1 h, followed by 10 μM Kang-CES2 for 4 h; (f) C643 cells+1 mM LPA for 1 h, followed by 10 μM Kang-CES2 for 4 h; (B) Fluorescence intensity of different treatments in (A) (t test; ****, p < 0.0001). The error bar represents calculating the mean ±SEM in three measurements. λ_{ex} = 450 nm, λ_{em} = 600–800 nm.

The results also showed that the fluorescence intensity of C643 cells was significantly higher than that of Nthy-ori3–1 cells, indicating that the content of CES2 in C643 cells was higher than that of Nthy-ori3–1 cells. It demonstrates the imaging capability of the probe in the cellular microenvironment. After adding enzyme activator 5-FU, the fluorescence intensity of C643 cells (e) was significantly improved. Subsequently, we noticed that the fluorescence intensity of the C643 cells (f) decreased significantly after adding enzyme inhibitor LPA. These results confirm that the intracellular action of Kang-CES2 is directly related to the content of CES2, and the fluorescence intensity can reflect the content of CES2.

3.5. Visualization of endogenous CES2 in vivo

In view of the ability of Kang-CES2 to visualize CES2 in vitro was satisfactory, we further imaged endogenous CES2 in vivo. The tumor of C643 tumor-bearing mice was injected with Kang-CES2 and imaged at various periods of time (Fig. 5A). The fluorescence appeared in the tumor of C643 tumor-bearing mice as early as 15 min, and the fluorescence intensity gradually increased over time, reaching a peak at 60 min, and then gradually weakening. It is worth noting that the imaging time covers the duration of most thyroid surgeries and can support the completion of thyroid surgery[57]. The fluorescence intensity of C643 tumor tissue is much higher than that of other normal tissues, which indicates that Kang-CES2 has excellent in vivo imaging ability. Subsequently, to further investigate the tissue imaging capabilities of Kang-CES2, we performed fluorescence imaging of C643 tumor-bearing mouse organs using spray (Fig. 5C). Fluorescence imaging results showed that C643 tumor tissue could be accurately distinguished from normal tissue after 30 minutes of spraying. These results also further
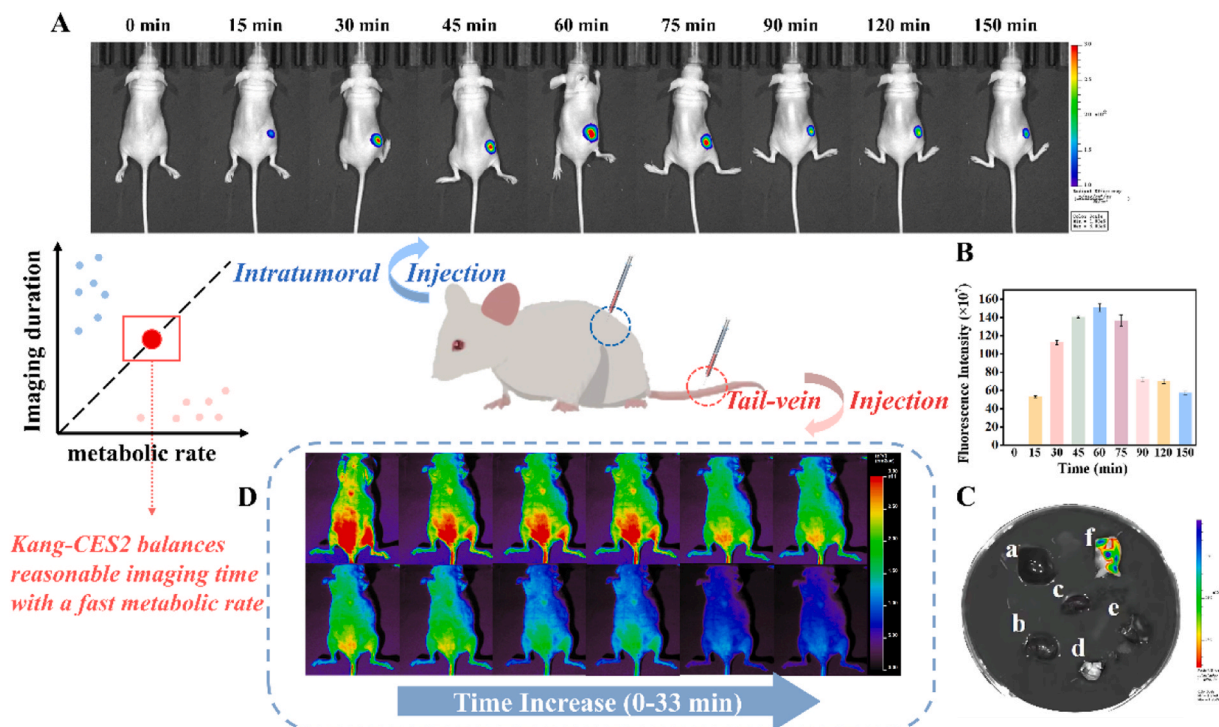

Fig. 5. (A) Fluorescence images of CES2 in intratumor injection of Kang-CES2 (200 μM, 100 μL) in C643 tumor-bearing mice captured at different times; (B) changes in fluorescence over time at the C643 tumor site in (A); (C) fluorescent images of major internal organs and C643 tumor tissue (a. liver; b. heart; c. spleen; d. lung; e. kidney; f. muscle tissue containing C643 tumor tissue); (D) fluorescence imaging of normal mice by tail-vein injection at different times (Kang-CES2, 200 μM, 300 μL). λ_{ex} = 450 nm, λ_{em} = 600–800 nm.

suggest that Kang-CES2 can be used to locate cancerous tissue using a spray method during surgery and as an imaging tool for C643 tumor biopsies.

Kang-CES2 has a tendency to reduce fluorescence in tumors and shows good photostability in spectral and cell experiments, which inspires us to explore whether Kang-CES2 can be naturally metabolized in vivo. We gave normal mice a tail-vein injection (Fig. 5D). CES2 is reported to be present in many organs in the abdomen of mice. Strong fluorescence signals appear soon after Kang-CES2 injection (about 5 minutes). With the increase of time, the fluorescence intensity in mice decreased gradually (basically no fluorescence in the body for about 33 minutes). In conclusion, Kang-CES2 can respond to CES2 in mice and finally be excreted rapidly with metabolism in vivo. These results suggest that ATC tissue can be surgically removed by intratumoral injection of Kang-CES2 during ATC surgery, and the remainder can be excreted by rapid metabolism in the body. Kang-CES2 has the potential to be used as a minimally invasive intraoperative imaging tool with rapid metabolism.

4. Conclusion

We designed and synthesized of a rapidly metabolizable NIR fluorescent probe Kang-CES2 based on isophorone for enzyme-activated imaging ATC in vivo, which has good photostability, selectivity, low cytotoxicity and good biosafety. The experimental results show that Kang-CES2 can respond specifically to CES2 in vitro and in vivo, and then emit NIR light. The sensing mechanism of Kang-CES2 to CES2 was investigated by HPLC analysis, LC-HRMS analysis, CV test and molecular docking simulation. Through the experimental results of the above tests, we demonstrated that CES2 can cut the ester bond of Kang-CES2 and restore it to fluorophore DIPCl-OH. In cell imaging, Kang-CES2 can distinguish between normal cells and C643 cells by fluorescence imaging. Kang-CES2 also demonstrates excellent imaging capabilities in vivo imaging and its potential as a spray tool and biopsies tool. The results of intratumoral injection in mice showed that Kang-CES2 can quickly distinguish between normal and ATC tissues and continue to emit NIR light within a reasonable time required for surgery. In addition, by injecting Kang-CES2 into the tail vein of mice, imaging results showed that Kang-CES2 can be rapidly metabolized from the body (the whole process is 33 minutes) without accumulation in the organism. The performance of Kang-CES2 achieves the balance of imaging ATC tissue at a reasonable time and metabolism rate. We believe Kang-CES2 has the potential to be a powerful fluorescent tool capable of guiding ATC surgical resection with rapid metabolism.

CRediT authorship contribution statement

Yuning Wang: Software, Formal analysis. **Jingkang Li:** Investigation, Data curation. **Lanlan Xu:** Investigation, Data curation. **Pinyi Ma:** Writing – review & editing, Software, Project administration, Data curation, Conceptualization. **Daqian Song:** Software, Resources, Investigation. **ying sun:** Writing – review & editing, Supervision, Resources, Project administration, Funding acquisition. **Wenxin Kang:** Writing – original draft, Validation, Investigation, Data curation, Conceptualization. **Mo Ma:** Investigation, Data curation. **Shuai Tang:** Investigation, Data curation.

Declaration of Competing Interest

The authors declare that they have no known competing financial interests or personal relationships that could have appeared to influence the work reported in this paper.

Data availability

Data will be made available on request.

Appendix A. Supporting information

Supplementary data associated with this article can be found in the online version at doi:10.1016/j.snb.2024.136299.

References

[1] H. Wu, S.C. Alexander, S. Jin, N.K. Devaraj, A bioorthogonal near-infrared fluorogenic probe for mRNA detection, J. Am. Chem. Soc. 138 (2016) 11429–11432.

[2] P. Cheng, J. Zhang, J. Huang, Q. Miao, C. Xu, K. Pu, Near-infrared fluorescence probes to detect reactive oxygen species for keloid diagnosis, Chem. Sci. 9 (2018) 6340–6347.

[3] D. Su, C.L. Teoh, S.-J. Park, J.-J. Kim, A. Samanta, R. Bi, et al., Seeing elastin: a near-infrared zwitterionic fluorescent probe for in vivo elastin imaging, Chem 4 (2018) 1128–1138.

[4] T.W.J. Gadella, New near-infrared fluorescent probes and tools, Nat. Methods 19 (2022) 654–655.

[5] C. Ding, T. Ren, Near infrared fluorescent probes for detecting and imaging active small molecules, Coord. Chem. Rev. 482 (2023) 215080.

[6] X.-F. Zhang, L. Shen, S. Wang, Q. Chen, X.-Q. Cao, S.-L. Shen, et al., A new xanthene-based platform for developing NIR fluorogenic probes for in vivo bioimaging, Chem. Eng. J. 472 (2023) 145065.

[7] F. Ding, J. Feng, X. Zhang, J. Sun, C. Fan, Z. Ge, Responsive optical probes for deep-tissue imaging: photoacoustics and second near-infrared fluorescence, Adv. Drug Deliv. Rev. 173 (2021) 141–163.

[8] J. Huang, K. Pu, Near-infrared fluorescent molecular probes for imaging and diagnosis of nephro-urological diseases, Chem. Sci. 12 (2021) 3379–3392.

[9] S. Feng, J. Zheng, J. Zhang, Z. Gui, G. Feng, Fe2+ imaging in ferroptosis and drug-induced liver injury with a ratiometric near-infrared fluorescent probe, Sens. Actuators B Chem. 371 (2022) 132512.

[10] J. Hong, Y. Liu, X. Tan, G. Feng, Engineering of a NIR fluorescent probe for high-fidelity tracking of lipid droplets in living cells and nonalcoholic fatty liver tissues, Biosens. Bioelectron. 240 (2023) 115646.

[11] J. Hong, Q. Li, Q. Xia, G. Feng, Real-time and high-fidelity tracking of lysosomal dynamics with a dicyanoisophorone-based fluorescent probe, Anal. Chem. 93 (2021) 16956–16964.

[12] S. Gong, J. Hong, E. Zhou, G. Feng, A near-infrared fluorescent probe for imaging endogenous carbon monoxide in living systems with a large Stokes shift, Talanta 201 (2019) 40–45.

[13] J. Hong, W. Feng, G. Feng, Highly selective near-infrared fluorescent probe with rapid response, remarkable large Stokes shift and bright fluorescence for H2S detection in living cells and animals, Sens. Actuators B Chem. 262 (2018) 837–844.

[14] F. Yuan, X. He, Y. Lu, L. Ning, X. Zhao, S. Zhang, et al., Photoactivated hydrogen sulfide donor with a near-infrared fluorescence report system for accelerated chronic wound healing, Anal. Chem. 95 (2023) 6931–6939.

[15] T. Wang, S. Wang, Z. Liu, Z. He, P. Yu, M. Zhao, et al., A hybrid erbium(III)–bacteriochlorin near-infrared probe for multiplexed biomedical imaging, Nat. Mater. 20 (2021) 1571–1578.

[16] G. Fürtjes, M. Weitzenberg, B. Arús, H. Rolbieski, C. Mawrin, R. Goldbrunner, et al., KS04.5.A Development of a somatostatin receptor type 2 (SSTR2)-targeted probe for near infrared fluorescence guided meningioma surgery, Neuro-Oncol. 24 (2022) ii5.

[17] Y. Sun, X. Zeng, Y. Xiao, C. Liu, H. Zhu, H. Zhou, et al., Novel dual-function near-infrared II fluorescence and PET probe for tumor delineation and image-guided surgery, Chem. Sci. 9 (2018) 2092–2097.

[18] L. Fu, Y. Tan, Y. Ding, W. Qing, Y. Wang, Water–soluble and polarity–sensitive near–infrared fluorescent probe for long–time specific cancer cell membranes imaging and C. Elegans label, Chin. Chem. Lett. 35 (2024) 108886.

[19] C. Li, Y. Wang, S. Huang, X. Zhang, X. Kang, Y. Sun, et al., A photostable fluorescent probe for long-time imagining of lysosome in cell and nematode, Talanta 188 (2018) 316–324.

[20] L. Xu, H. Chu, D. Gao, Q. Wu, Y. Sun, Z. Wang, et al., Chemosensor with ultra-high fluorescence enhancement for assisting in diagnosis and resection of ovarian cancer, Anal. Chem. 95 (2023) 2949–2957.

[21] Y. Wang, Y. Zhang, M. Li, X. Gao, D. Su, An efficient strategy for constructing fluorescent nanoprobes for prolonged and accurate tumor imaging, Anal. Chem. 96 (2024) 2481–2490.

[22] L. Zhang, J.-L. Wang, X.-X. Ba, S.-Y. Hua, P. Jiang, F.-L. Jiang, et al., Multifunction in one molecule: mitochondrial imaging and photothermal & photodynamic cytotoxicity of fast-response near-infrared fluorescent probes with aggregation-induced emission characteristics, ACS Appl. Mater. Interfaces 13 (2021) 7945–7954.

[23] X. Luo, D. Hu, D. Gao, Y. Wang, X. Chen, X. Liu, et al., Metabolizable near-infrared-ii nanoprobes for dynamic imaging of deep-seated tumor-associated macrophages in pancreatic cancer, ACS Nano 15 (2021) 10010–10024.

[24] X. Luo, S. Cheng, W. Zhang, K. Dou, R. Wang, F. Yu, Near-infrared fluorescence probe for indication of the pathological stages of wound healing process and its clinical application, ACS Sens. 9 (2024) 810–819.

[25] P. Gao, H. Hui, C. Guo, Y. Liu, Y. Su, X. Huang, et al., Renal clearing carbon dots-based near-infrared fluorescent super-small nanoprobe for renal imaging, Carbon 201 (2023) 805–814.

[26] T. Xue, Y. Dai, X. Zhang, Y. Cheng, X. Gu, H. Ji, et al., Ultrasensitive near-infrared fluorescent probe with large stokes shift for real-time tracing of CYP1A1 in living cells and zebrafish model, Sens. Actuators B Chem. 293 (2019) 265–272.

[27] J. Zhan, W. Song, E. Ge, L. Dai, W. Lin, Reversible fluorescent probes for biological dynamic imaging: Current advances and future prospects, Coord. Chem. Rev. 493 (2023) 215321.

[28] Y. Wang, J. Weng, X. Wen, Y. Hu, D. Ye, Recent advances in stimuli-responsive in situ self-assembly of small molecule probes for in vivo imaging of enzymatic activity, Biomater. Sci. 9 (2021) 406–421.

[29] R. Yan, Y. Hu, F. Liu, S. Wei, D. Fang, A.J. Shuhendler, et al., Activatable NIR fluorescence/MRI bimodal probes for in vivo imaging by enzyme-mediated fluorogenic reaction and self-assembly, J. Am. Chem. Soc. 141 (2019) 10331–10341.

[30] J. Zheng, Y. Xu, L. Fan, S. Qin, H. Li, M. Sang, et al., A bioresponsive near-infrared fluorescent probe for facile and persistent live-cell tracking, Small 16 (2020) 2002211.

[31] Y.-L. Qi, Y.-Z. Li, M.-J. Tan, F.-F. Yuan, N. Murthy, Y.-T. Duan, et al., Recent advances in organic near-infrared ratiometric small-molecule fluorescent probes, Coord. Chem. Rev. 486 (2023) 215130.

[32] W.-J. Fu, J.T. Li, W.H. Qian, X.Y. Zhang, D.D. Ma, Y.T. Wang, et al., Viscosity-triggered near-infrared fluorescence nanoprobe for in vivo non-invasive diagnosis of cancer, Chem. Eng. J. 464 (2023) 142521.

[33] G. Pellegriti, F. Frasca, C. Regalbuto, S. Squatrito, R. Vigneri, Worldwide increasing incidence of thyroid cancer: update on epidemiology and risk factors, J. Cancer Epidemiol. 2013 (2013) 965212.

[34] S.A. Khan, B. Ci, D.E. Gerber, D.G. McFadden, M.S. Beg, Y. Xie, et al., Comprehensive genomic sequencing (CGS) of 90 patient samples of anaplastic thyroid cancer (ATC), J. Clin. Oncol. 34 (2016) 6014.

[35] K.M. Gallagher, P.A. Haddad, D.A. Hammoud, Comparative efficacy of primary treatment approaches in anaplastic thyroid carcinoma (ATC): an updated network meta-analysis, J. Clin. Oncol. 38 (2020) e18566.

[36] A.A. Kühl, U. Erben, C. Cieluch, S. Spieckermann, J. Gröne, P. Lohneis, et al., Tissue-infiltrating plasma cells are an important source of carboxylesterase 2 contributing to the therapeutic efficacy of prodrugs, Cancer Lett. 378 (2016) 51–58.

[37] S.E. Pratt, S. Durland-Busbice, R.L. Shepard, K. Heinz-Taheny, P.W. Iversen, A. H. Dantzig, Human carboxylesterase-2 hydrolyzes the prodrug of gemcitabine (LY2334737) and confers prodrug sensitivity to cancer cells, Clin. Cancer Res. 19 (2013) 1159–1168.

[38] D. Wang, L. Zou, Q. Jin, J. Hou, G. Ge, L. Yang, Human carboxylesterases: a comprehensive review, Acta Pharm. Sin. B 8 (2018) 699–712.

[39] B.L. Barthel, Z. Zhang, D.L. Rudnicki, C.D. Coldren, M. Polinkovsky, H. Sun, et al., Preclinical efficacy of a carboxylesterase 2-activated prodrug of doxazolidine, J. Med. Chem. 52 (2009) 7678–7688.

[40] X. Chen, Q. Liu, Y. Chen, L. Wang, R. Yang, W. Zhang, et al., Carboxylesterase 2 induces mitochondrial dysfunction via disrupting lipid homeostasis in oral squamous cell carcinoma, Mol. Metab. 65 (2022) 101600.

[41] K. Kailass, O. Sadovski, M. Capello, Ya Kang, J.B. Fleming, S.M. Hanash, et al., Measuring human carboxylesterase 2 activity in pancreatic cancer patient-derived xenografts using a ratiometric fluorescent chemosensor, Chem. Sci. 10 (2019) 8428–8437.

[42] Y. Li, M. Zalzala, K. Jadhav, Y. Xu, T. Kasumov, L. Yin, et al., Carboxylesterase 2 prevents liver steatosis by modulating lipolysis, endoplasmic reticulum stress, and lipogenesis and is regulated by hepatocyte nuclear factor 4 alpha in mice, Hepatology 63 (2016).

[43] S.-Y. Liu, X. Zou, Y. Guo, X. Gao, A highly sensitive and selective enzyme activated fluorescent probe for in vivo profiling of carboxylesterase 2, Anal. Chim. Acta 1221 (2022) 340126.

[44] Y.-Q. Song, X.-Q. Guan, Z.-M. Weng, Y.-Q. Wang, J. Chen, Q. Jin, et al., Discovery of a highly specific and efficacious inhibitor of human carboxylesterase 2 by large-scale screening, Int. J. Biol. Macromol. 137 (2019) 261–269.

[45] H.-Z. Sun, G.-Q. Qin, F.-G. Wang, Y. Bai, Z. Zhang, Z.-Z. Fang, Hydroxylated polychlorinated biphenyls (OH-PCBs) exert strong inhibitory effects towards human carboxylesterases (CESs), Sci. Total Environ. 745 (2020) 141140.

[46] X. Tian, F. Yan, J. Zheng, X. Cui, L. Feng, S. Li, et al., Endoplasmic reticulum targeting ratiometric fluorescent probe for carboxylesterase 2 detection in drug-induced acute liver injury, Anal. Chem. 91 (2019) 15840–15845.

[47] L. Feng, P. Li, J. Hou, Y.-L. Cui, X.-G. Tian, Z.-L. Yu, et al., Identification and isolation of glucosytransferases (GT) expressed fungi using a two-photon ratiometric fluorescent probe activated by GT, Anal. Chem. 90 (2018) 13341–13347.

[48] R. Li, F. Xue, C. Cao, P. Wei, Y. Zhong, S. Xiao, et al., A near infrared fluorescent probe for one-step detection of histone deacetylase activity based on an intramolecular FRET, Sens. Actuators B Chem. 297 (2019) 126791.

[49] Y. Wang, L. Chen, Smart fluorescent probe strategy for precision targeting hypoxic tumor, J. Med. Chem. 64 (2021) 2967–2970.

[50] G. Xu, W. Zhang, M.K. Ma, H.L. McLeod, Human carboxylesterase 2 is commonly expressed in tumor tissue and is correlated with activation of irinotecan1, Clin. Cancer Res. 8 (2002) 2605–2611.

[51] S.J. Park, Y.J. Kim, J.S. Kang, I.Y. Kim, K.S. Choi, H.M. Kim, Carboxylesterase-2-selective two-photon ratiometric probe reveals decreased carboxylesterase-2 activity in breast cancer cells, Anal. Chem. 90 (2018) 9465–9471.

[52] X. Wang, J. Gao, C. Fan, Y. Gao, X. Yang, L. Chen, New near-infrared fluorescence imaging platform with large stokes shift for carboxylesterase 2 detection in thyroid cancer and inflammatory diseases diagnosis, Anal. Chem. 96 (2024) 3772–3779.

[53] X. Luo, R. Wang, C. Lv, G. Chen, J. You, F. Yu, Detection of selenocysteine with a ratiometric near-infrared fluorescent probe in cells and in mice thyroid diseases model, Anal. Chem. 92 (2020) 1589–1597.

[54] W. Kang, M. Ma, L. Xu, S. Tang, J. Li, P. Ma, et al., Customized fluorescent probe for peering into the expression of butyrylcholinesterase in thyroid cancer, Anal. Chim. Acta 1282 (2023) 341932.

[55] J. Li, M. Ma, J. Li, L. Xu, D. Song, P. Ma, et al., Visualizing dipeptidyl peptidase-IV with an advanced non-π-conjugated fluorescent probe for early thyroid disease diagnosis, Anal. Chem. 95 (2023) 17577–17585.

[56] L. Xu, M. Ma, J. Li, D. Dai, D. Gao, P. Ma, et al., Exploration of aminopeptidase N as new biomarker for early diagnosis of thyroid cancer, Biosens. Bioelectron. 244 (2024) 115808.

[57] M.-Y. Lee, J.-D. Wang, C.-W. Tu, C.-C. Alex Tseng, Operation time is a major risk factor on postoperative nausea and vomiting in women undergoing breast and thyroid surgery, Asian J. Surg. 44 (2021) 590–591.

Wenxin Kang is currently a master degree student in College of Chemistry, Jilin University. Her interest is spectral analysis.

Mo Ma is currently a Ph.D. student in College of Chemistry, Jilin University. His interest is spectral analysis.

Shuai Tang is currently a Ph.D. student in College of Chemistry, Jilin University. His interest is spectral analysis.

Yuning Wang is currently a master degree student in College of Chemistry, Jilin University. Her interest is spectral analysis.

Jingkang Li is currently a Ph.D. student in College of Chemistry, Jilin University. Her interest is spectral analysis.

Lanlan Xu is currently a Ph.D. student in College of Chemistry, Jilin University. Her interest is spectral analysis.

Pinyi Ma gained his doctor's degree from College of Chemistry, Jilin University in 2017 and he is an associate professor in that school. His research area is spectral analysis.

Daqian Song gained his doctor's degree from College of Chemistry, Jilin University in 2003 and he is a professor in that school. His research areas are spectral and chromatography analysis.

Ying Sun gained his doctor's degree from College of Chemistry, Jilin University in 2009 and she is a professor in that school. His research area is spectral analysis.